Phys. Biol. **6** (2009) 046002 (15pp) doi:10.1088/1478-3975/6/4/046002

# Modeling the slowing of neurofilament transport along the mouse sciatic nerve

**P Jung**[1] **and A Brown**[2]

[1] Department of Physics and Astronomy and Quantitative Biology Institute, Ohio University, Athens, OH 45701, USA
[2] Center for Molecular Neurobiology and Department of Neuroscience, The Ohio State University, Columbus, OH 43210, USA

Received 6 April 2009
Accepted for publication 7 July 2009
Published 21 August 2009
Online at stacks.iop.org/PhysBio/6/046002

**Abstract**
Neurofilaments are transported along axons in the slow component of axonal transport. The average rate of movement is generally quoted as several millimeters or tenths of a millimeter per day, but this rate is known to decrease while the neurofilaments are in transit due to spatial and temporal factors that are not understood. We have previously presented a stochastic model for neurofilament movement *in vivo* based on the transport kinetics of single neurofilaments observed by time-lapse fluorescence imaging in cultured neurons. The model took into account multiple velocity states and was only accessible through computational simulations. In simulations of the movement of a pulse of radiolabeled neurofilaments, this model generated a Gaussian wave which closely matched the experimental data. Here we present a simpler model with only three velocity states which is more amenable to analytical approaches. We show that the transport wave can be fully described by the mean and variance and we present analytical solutions for these cumulants in terms of the kinetic parameters of the model. We use the resulting expressions to examine the slowing of neurofilament transport in the mouse sciatic nerve. We show that the slowing is accompanied by an increase in the spread of the wave and that these changes are most readily explained by a change in the rate at which neurofilaments reverse their direction of movement. This suggests that the directionality of neurofilament transport in axons may be under spatial and/or temporal control and that alterations in the directionality of neurofilament transport could provide a mechanism for regulating the transport and distribution of these cytoskeletal polymers along axons.

## 1. Slow axonal transport

Many axonal macromolecules and organelles are manufactured in the neuronal cell body and shipped out along the axon by a process called axonal transport. Membranous organelles move rapidly and continuously, at average velocities of approximately 100–400 mm/day (fast axonal transport), whereas cytoskeletal polymers and cytosolic macromolecular complexes move much more slowly, at average velocities of approximately 0.2–8 mm/day (slow axonal transport) [1, 2]. Among the slowest of these cargoes are the neurofilaments, which move at average velocities of approximately 0.2–3 mm/day [3, 4]. Studies on the axonal transport of neurofilaments *in vivo* using radioisotopic pulse labeling have shown that the pulse of radiolabeled neurofilament proteins forms a unimodal bell-shaped wave that spreads as it moves distally. The average velocity is generally quoted as the rate of movement of the peak of the wave, but the spreading of the wave indicates that the polymers move at a broad range of rates.

Neurofilament movement can be observed directly in cultured nerve cells by transfection with fusion proteins composed of a neurofilament protein linked to a fluorescent protein. The fluorescent neurofilament fusion proteins coassemble with endogenous neurofilament proteins to make fluorescent neurofilaments, which can be observed by time-lapse fluorescence microscopy [5]. Studies using this approach have shown that (1) axonal neurofilament proteins move in the form of assembled neurofilament polymers [6], (2) axonal neurofilaments move rapidly, approaching the rate of fast

 

**Table 1.** Summary of experimental data on neurofilament movement obtained in cultured neurons from neonatal rat and mouse superior cervical ganglia. The velocities are time-weighted average interval velocities; they differ slightly from previously reported values, which were weighted according to filament number. The rat data are from the published study of Wang and Brown [9]. The mouse data are from the unpublished study of Uchida *et al* [38].

| | Rat superior cervical ganglion neuron | | Mouse superior cervical ganglion neuron | |
|---|---|---|---|---|
| | Anterograde | Retrograde | Anterograde | Retrograde |
| Average velocity | 0.53 $\mu$m s$^{-1}$ | −0.6 $\mu$m s$^{-1}$ | 0.51 $\mu$m s$^{-1}$ | −0.52 $\mu$m s$^{-1}$ |
| Number of filaments tracked | 50 | 22 | 93 | 103 |
| Direction of movement | 69% | 31% | 47% | 53% |
| Average frequency of movement | 0.15 filaments min$^{-1}$ | | 0.22 filaments min$^{-1}$ | |
| Average time pausing | 67% | | 68% | |
| Pause cutoff | 0.0685 $\mu$m s$^{-1}$ | | 0.131 $\mu$m s$^{-1}$ | |
| Time intervals | 4 s or 5 s | | 4 s | |
| Number of movies analyzed | 76 | | 61 | |
| Average movie duration | 6.38 min | | 14.5 min | |
| Total observation time | 484.6 min | | 884.7 min | |

axonal transport, but their movements are also intermittent and highly asynchronous [7–9], and (3) axonal neurofilaments move in both directions, but reversals are infrequent [10]. Further studies using a fluorescence photoactivation pulse-escape technique have shown that axonal neurofilaments switch between two distinct kinetic states: a mobile state, in which they alternate between bouts of rapid movement and short pauses, and a stationary state, in which they pause for prolonged periods with no movement [11]. We have termed these states 'on-track' and 'off-track', respectively, and we proposed that they may differ in the proximity or engagement of the neurofilaments with the microtubule tracks along which they move. In cultured rat superior cervical ganglion neurons, the average pause duration was 29 s in the mobile state and 61 min in the stationary state.

The motile behavior of neurofilaments in cultured nerve cells suggests that slow axonal transport is the result of rapid bidirectional movements interrupted by prolonged pauses [2, 12]. Whether the movement is considered slow or fast depends on the timescale of observation. To test this 'stop-and-go' hypothesis, we previously developed a computational model of slow axonal transport based on our time-lapse imaging data [13]. To characterize neurofilament movement, we calculated the velocity for each time interval and then binned these interval velocities into seven distinct velocity states. We then calculated the frequency with which neurofilaments transitioned between these seven states in successive time intervals. The resulting frequencies were used to generate a seven-by-seven matrix of transition probabilities which we used to simulate the movement of neurofilaments *in silico*. While this approach provided insight into the transport process, it is problematic for two reasons. First, very large numbers of neurofilaments must be tracked to obtain statistical confidence in the transition probabilities, especially for the higher velocity bins which are typically not heavily populated. Second, the choice of the number and size of the velocity bins is arbitrary. In this paper, we present a more rational model based on only three velocity states (pausing, moving anterograde and moving retrograde). The resulting model is more compact than the previous model, enabling us to derive explicit expressions for the velocity and spreading of the transport wave. These expressions allow us to predict neurofilament transport *in vivo* on a timescale of days and weeks based on parameters derived from direct observations in cultured neurons on a timescale of seconds and minutes.

One feature of neurofilament transport *in vivo* that has not received much attention is that the transport rates frequently slow along the length of the axon [14–17]. One study which examined this phenomenon systematically concluded that it is influenced by both spatial factors (i.e. distance along the nerve) and temporal factors (i.e. time elapsed) [15]. There is evidence that this slowing may be caused by neurofilament phosphorylation [18–21], but this has not been proven. Here, we use our modeling approach to investigate the mechanism of slowing of neurofilament transport in mouse sciatic nerve. We find that the decrease in velocity in the radioisotopic pulse labeling experiments is accompanied by an increase in the spreading of the transport wave. We show that these changes are most likely due to changes in the frequency with which neurofilaments reverse their direction of movement. This suggests that the directionality of neurofilament transport in axons may be under spatial and/or temporal control and that alterations in the directionality of neurofilament transport could provide a mechanism for regulating the transport and distribution of these cytoskeletal polymers along axons.

## 2. Experimental measurements

To record neurofilament movement, cultured neurons were transfected with GFP-tagged neurofilament protein and the movement of fluorescent neurofilaments was tracked through naturally occurring or photobleached gaps in the axonal neurofilament array by time-lapse fluorescence microscopy as previously described [5]. The data on rat superior cervical ganglion neurons were obtained from our published work on photobleached gaps [9] whereas the data on mouse superior cervical ganglion neurons were obtained from our unpublished work on naturally occurring gaps [38] (table 1). The time-lapse intervals $\delta t$ were 4 s or 5 s, and the position of the

filament in each frame was defined as the position of its leading end. A recording started when a neurofilament entered a gap and it ended when it departed. The on- and off-track rate constants, which dictate the long-term pausing behavior of the neurofilaments, were obtained from our published work on rat superior cervical ganglion neurons using the fluorescence photoactivation pulse-escape strategy mentioned above [11].

## 3. Model development

In this section, we develop step by step a mathematical model of neurofilament movement in axons based on our observations of neurofilament movement in cultured neurons. Our model differs significantly from the original model of Blum and Reed [22], published 20 years ago, in that it builds directly on our experimental measurements of the movement of single neurofilaments. The basic assumptions of our model are as follows: (1) neurofilaments move linearly along the long axis of the axon, (2) the neurofilaments either pause, move in the *anterograde* direction with velocity $v_a$ or move in the *retrograde* direction with velocity $v_r$, (3) the behavior of each neurofilament is independent of its neighbors, and (4) all neurofilaments behave in a statistically identical manner. In contrast to our previous approach [13], but similar to the approach of Craciun *et al* [23], we define just three velocity states: one anterograde velocity $v_a$, one retrograde velocity $v_r$ and zero velocity (pausing). This simpler scheme is less arbitrary and more tractable mathematically. The anterograde and retrograde velocities, $v_a$ and $v_r$ respectively, are defined as the average anterograde and retrograde velocities excluding pauses. To distinguish movements from pauses, we define a velocity cutoff, $v_c$, which represents the magnitude of displacement that constitutes a movement; any movement that is slower than this cutoff is considered to be a pause. As we have described in previous studies, we set $v_c$ to be one camera pixel per second, which corresponds to $v_c = 0.065\ \mu\text{m s}^{-1}$ for the rat superior cervical ganglion neuron data and $v_c = 0.13\ \mu\text{m s}^{-1}$ for the mouse superior cervical ganglion neuron data (table 1).

### 3.1. Transition probabilities

We first consider a two-state model in which the neurofilaments move unidirectionally and switch between a moving and a pausing state (see figure 1). We define the probability that a moving neurofilament transitions to the pausing state within a time interval of $\delta t$ as $p_{\delta t}(1|0)$, and thus the probability that a moving neurofilament remains in the moving state is given by $p_{\delta t}(1|1) = 1 - p_{\delta t}(1|0)$. Similarly, we define the probability that a pausing neurofilament transitions to the moving state as $p_{\delta t}(0|1)$, and thus the probability that a pausing neurofilament remains in the pausing state is given by $p_{\delta t}(0|0) = 1 - p_{\delta t}(0|1)$. To obtain these transition probabilities from our time-lapse movies, we calculate a velocity for each time interval for every filament tracked, and then we use the velocity cutoff $v_c$, described above, to define these time intervals as either movements or pauses. We then take the fraction of the total number of time intervals corresponding to each transition

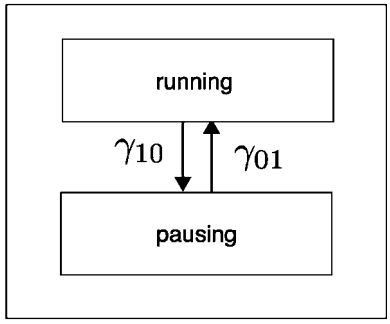


**Figure 1.** The kinetic scheme of neurofilament transport for a simple two-state model in which the filaments can either move or pause.

(pause to pause, move to move, move to pause and pause to move) to be the probability associated with that transition. Since our previous studies revealed no apparent difference between the moving and pausing behavior of anterograde and retrograde filaments [7, 9], at least within the axon proper, we lump the anterograde and retrograde data together to generate a single transition probability matrix. For the rat superior cervical ganglion neuron data set, the resulting transition probability matrix is given by

$$\mathbf{p} = \begin{pmatrix} p_{\delta t}(0|0) & p_{\delta t}(0|1) \\ p_{\delta t}(1|0) & p_{\delta t}(1|1) \end{pmatrix} = \begin{pmatrix} 0.85 & 0.15 \\ 0.33 & 0.67 \end{pmatrix}, \tag{1}$$

whereas for the mouse superior cervical ganglion neuron data set, it is given by

$$\mathbf{p} = \begin{pmatrix} p_{\delta t}(0|0) & p_{\delta t}(0|1) \\ p_{\delta t}(1|0) & p_{\delta t}(1|1) \end{pmatrix} = \begin{pmatrix} 0.82 & 0.18 \\ 0.38 & 0.62 \end{pmatrix}. \tag{2}$$

From these transition probability matrices, we infer the actual rate constants $\gamma_{ij}$ by using the underlying two-state rate equations:

$$\begin{aligned} \frac{\mathrm{d}p_0}{\mathrm{d}t} &= -\gamma_{01} p_0 + \gamma_{10} p_1 \\ \frac{\mathrm{d}p_1}{\mathrm{d}t} &= -\gamma_{10} p_1 + \gamma_{01} p_0, \end{aligned} \tag{3}$$

where $p_0$ and $p_1$ denote the probabilities of a neurofilament residing in the pausing or moving state, respectively. With $p_{\delta t}(0|1) = p_1(t)$ if $p_1(0) = 0$, and $p_{\delta t}(1|0) = p_0(t)$ if $p_0(0) = 0$, we find for the rates

$$\begin{aligned} \gamma_{01} &= -\frac{1}{\delta t} \frac{p_{\delta t}(0|1)}{p_{\delta t}(0|1) + p_{\delta t}(1|0)} \ln(1 - p_{\delta t}(0|1) - p_{\delta t}(1|0)) \\ \gamma_{10} &= -\frac{1}{\delta t} \frac{p_{\delta t}(1|0)}{p_{\delta t}(0|1) + p_{\delta t}(1|0)} \ln(1 - p_{\delta t}(0|1) - p_{\delta t}(1|0)). \end{aligned} \tag{4}$$

For the rat superior cervical ganglion neuron data set, we find

$$\begin{aligned} \gamma_{01} &= 0.041\ \text{s}^{-1} \\ \gamma_{10} &= 0.093\ \text{s}^{-1}, \end{aligned} \tag{5}$$

whereas for the mouse superior cervical ganglion neuron data set, we find

$$\begin{aligned} \gamma_{01} &= 0.064\ \text{s}^{-1} \\ \gamma_{10} &= 0.14\ \text{s}^{-1}. \end{aligned} \tag{6}$$

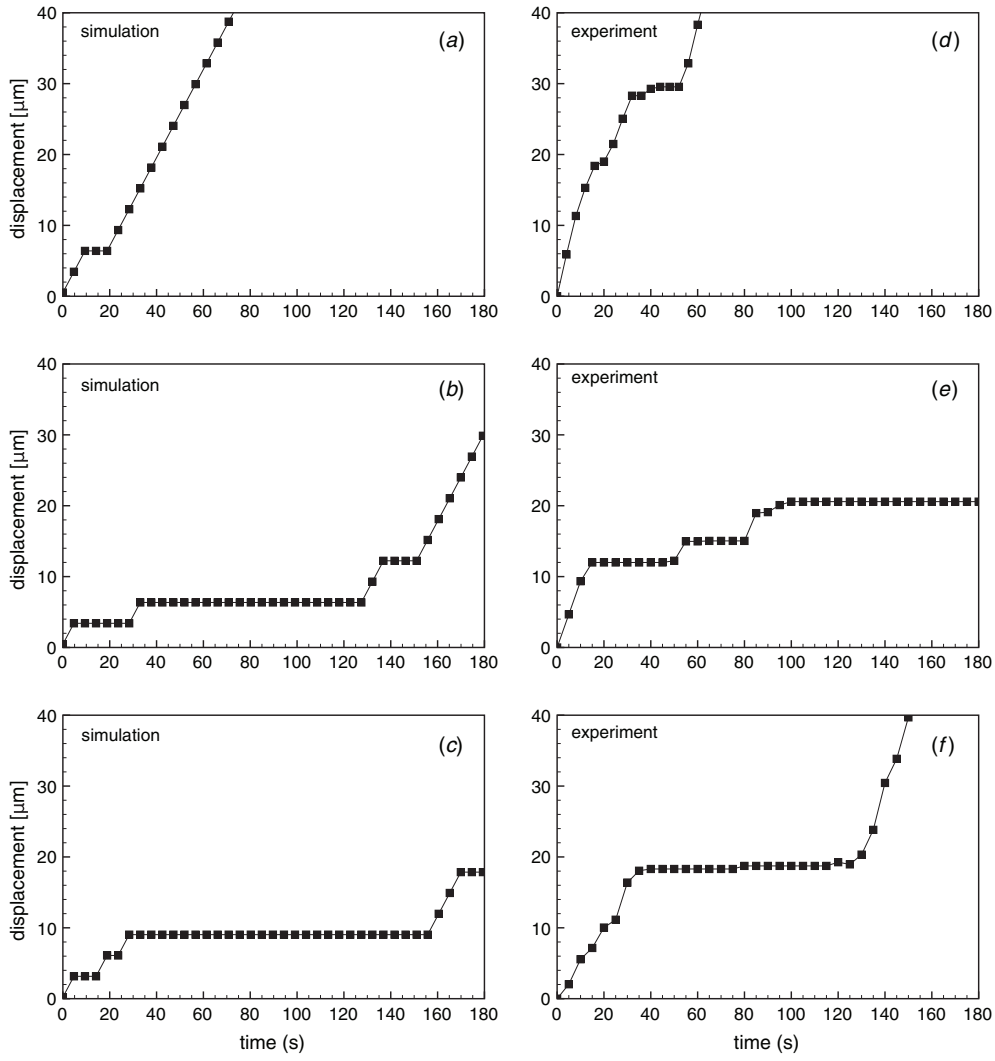


**Figure 2.** (*a*)–(*c*) Three excerpts from the *in silico* movement of a neurofilament generated by a Markov process with the transition probability matrix given in equation (1). (*d*)–(*f*) Three examples of neurofilament movement through photobleached gaps in the axonal neurofilament array of cultured rat superior cervical ganglion neurons from the published study of Wang and Brown [9].

### *3.2. Neurofilament movement*

To characterize the movement generated by the transition probability matrices calculated above, we run a stochastic simulation of neurofilament movement *in silico*. In order to mimic the experimental conditions, we track the filaments within a 70 $\mu$m window. Initially, we place the neurofilament 50 $\mu$m to the left of the window and allow it to move. We begin tracking its movement when it enters the window and we continue to track it until it reaches the other end of the window or until the time tracked exceeds 300 s. After the end of the recording, a new neurofilament is launched 50 $\mu$m to the left of the window and this process is repeated. Figure 2 shows movements generated using the transition probability matrix **p** obtained from the rat superior cervical ganglion neuron data set (equation (1)), compared to representative anterograde movements from the same experimental data set. The neurofilaments in the experimental data move in asynchronous bursts of rapid intermittent movement, as previously described. The *in silico* trajectories are coarser because there is just a single velocity of movement, but otherwise the overall behavior is similar.

To link the kinetics of single neurofilaments to spatial distributions of large *ensembles* of neurofilaments, such as encountered in experiments using radioisotopic pulse labeling [17], we use the following equations of motion:

$$\begin{aligned} \frac{\partial P_0}{\partial t} &= -\gamma_{01} P_0 + \gamma_{10} P_1 \\ \frac{\partial P_1}{\partial t} &= -v \frac{\partial P_1}{\partial x} - \gamma_{10} P_1 + \gamma_{01} P_0, \end{aligned} \tag{7}$$

where $P_1(x,t)$ and $P_0(x,t)$ are the probabilities of a neurofilament residing in the moving or pausing state, respectively, at time $t$ in the interval $[x : x+\mathrm{d}x]$. Alternatively, $P_1(x,t)$ and $P_0(x,t)$ can also be considered to represent the spatial distributions of an ensemble of independent neurofilaments in the moving or pausing states, respectively, at time $t$. Thus, since $P(x,t) \equiv P_1(x,t) + P_0(x,t)$ describes the spatial distribution of all neurofilaments (both moving and pausing), the average velocity is defined by

$$\bar{v} = \frac{\mathrm{d}}{\mathrm{d}t}\langle x(t)\rangle = \frac{\mathrm{d}}{\mathrm{d}t}\int_{-\infty}^{\infty} x\,P(x,t)\,\mathrm{d}x. \tag{8}$$

Taking the time derivative under the integral and using the equations of motion in equation (7), one readily finds

$$\bar{v} = v \int_{-\infty}^{\infty} P_1(x, t \to \infty)\, \mathrm{d}x = v \frac{1}{1+q_1}, \tag{9}$$

where $q_1 \equiv \frac{\gamma_{10}}{\gamma_{01}}$. Using the experimental data summarized in table 1, and taking the average velocity to be the average of all interval velocities excluding pauses (ignoring the direction of movement), we find $v = 0.55\ \mu\mathrm{m\ s^{-1}}$ and $v = 0.52\ \mu\mathrm{m\ s^{-1}}$ for the rat and mouse superior cervical ganglion neurons, respectively. Inserting these velocities into equation (9) along with the transition rates $\gamma_{01}$ and $\gamma_{10}$ given by equations (5) and (6), we find that $\bar{v} = 0.17\ \mu\mathrm{m\ s^{-1}}$ and $\bar{v} = 0.16\ \mu\mathrm{m\ s^{-1}}$ for the rat and mouse superior cervical ganglion neurons, respectively. In comparison, the average velocities calculated directly from our experimental data (again ignoring the direction of movement, but this time *including* pauses) are $\bar{v} = 0.18\ \mu\mathrm{m\ s^{-1}}$ and $0.17\ \mu\mathrm{m\ s^{-1}}$, respectively. The fact that these numbers are in close agreement supports the assumption made above in the development of our model that all neurofilaments behave in a statistically equivalent manner. It also shows that our model describes correctly the kinetic behavior of neurofilaments on fast timescales (i.e. tens of seconds or several minutes).

The movement and spatial distribution of ensembles of neurofilaments on slow timescales (days or weeks) have been characterized *in vivo* using radioisotopic pulse-labeling measurements. The initial pulse of radio-labeled neurofilaments assumes a bell-shaped distribution that spreads as it propagates along the axon in an anterograde direction. In stochastic simulations of radioisotopic pulse-labeling experiments, we showed previously that the bell-shaped wave appears to be a Gaussian [13]. In appendix A, we show that models of the type in equation (7) and more complex ones introduced below do indeed generate spatial distributions that approach Gaussians, and as such they can be fully characterized by the mean value ($\langle x(t)\rangle$) and the variance ($\sigma^2(t) \equiv \langle x^2\rangle - \langle x\rangle^2$), i.e.

$$P(x,t) = \frac{1}{\sqrt{2\pi\sigma^2(t)}} \exp\left(\frac{(x - \langle x(t)\rangle)^2}{2\sigma^2(t)}\right), \tag{10}$$

with mean value $\langle x(t)\rangle$ and variance $\sigma^2(t)$ linear in time. For the specific model in equation (7), we find

$$\begin{aligned}\frac{\mathrm{d}}{\mathrm{d}t}\sigma^2(t) &= \frac{\mathrm{d}}{\mathrm{d}t}\left(\int_{-\infty}^{\infty} x^2 P(x,t)\,\mathrm{d}x - \left(\int_{-\infty}^{\infty} x P(x,t)\,\mathrm{d}x\right)^2\right) \\ &= 2v^2 \frac{\gamma_{10}\gamma_{01}}{(\gamma_{01}+\gamma_{10})^3}.\end{aligned} \tag{11}$$

Using the transition probability matrices in equations (1) and (2), we calculate $\frac{\mathrm{d}}{\mathrm{d}t}\sigma^2(t) = 1.0\ \mu\mathrm{m}^2\ \mathrm{s}^{-1} = 0.087\ \mathrm{mm}^2/\mathrm{day}$ for the rat superior ganglion neuron data set and $\frac{\mathrm{d}}{\mathrm{d}t}\sigma^2(t) = 0.56\ \mu\mathrm{m}^2\ \mathrm{s}^{-1} = 0.048\ \mathrm{mm}^2/\mathrm{day}$ for the mouse superior cervical ganglion neuron data set.

The above calculations, of course, yield faster velocities and slower rates of spreading than observed for neurofilament transport *in vivo* because the model thus far assumes no off-track pauses and no retrograde movements. These additional levels of complexity will be incorporated into the model in the following sections. Also note that the diffusive profile of the pulse of neurofilaments, spreading with constant velocity, does not require a diffusion term in the master equation (7). The diffusive profile is generated by the random switching between mobile and immobile states of the neurofilament kinetics. Moreover, our experimental data indicate no significant diffusion of neurofilament polymers in axons [11], which is not surprising given their length and packing density within the axonal cytoplasm.

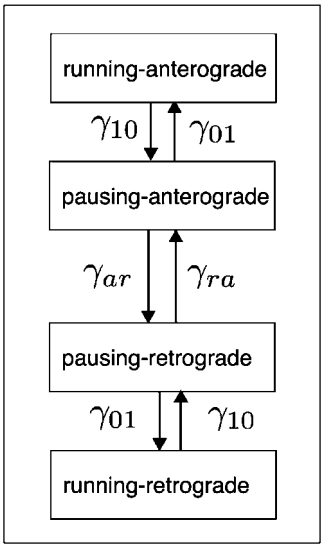


**Figure 3.** The kinetic scheme of neurofilament transport for a four-state model in which the filaments can move or pause in either an anterograde or a retrograde state.

### 3.3. Reversals

Up to now we have considered neurofilament movement to be exclusively anterograde. To account for bidirectional movement, we expand our model to include both anterograde and retrograde movements. We consider that the direction of movement is determined by the reversal rate constants $\gamma_{\mathrm{ar}}$ and $\gamma_{\mathrm{ra}}$ which define the rate of reversal from anterograde to retrograde and from retrograde to anterograde, respectively. We consider that the reversals can only occur when a filament is pausing [13], which is consistent with our observations of reversals in cultured neurons and with models of vesicular transport [24]. Hence, our expanded model now has four states (see figure 3) and is mathematically described by

$$\begin{aligned}\frac{\partial P_{\mathrm{a}}(x,t)}{\partial t} &= -v_{\mathrm{a}}\frac{\partial P_{\mathrm{a}}(x,t)}{\partial x} - \gamma_{10}P_{\mathrm{a}}(x,t) + \gamma_{01}P_{\mathrm{a0}}(x,t) \\ \frac{\partial P_{\mathrm{r}}(x,t)}{\partial t} &= -v_{\mathrm{r}}\frac{\partial P_{\mathrm{r}}(x,t)}{\partial x} - \gamma_{10}P_{\mathrm{r}}(x,t) + \gamma_{01}P_{\mathrm{r0}}(x,t) \\ \frac{\partial P_{\mathrm{a0}}(x,t)}{\partial t} &= -(\gamma_{01}+\gamma_{\mathrm{ar}})P_{\mathrm{a0}}(x,t) + \gamma_{10}P_{\mathrm{a}}(x,t) + \gamma_{\mathrm{ra}}P_{\mathrm{r0}}(x,t) \\ \frac{\partial P_{\mathrm{r0}}(x,t)}{\partial t} &= -(\gamma_{01}+\gamma_{\mathrm{ra}})P_{\mathrm{r0}}(x,t) + \gamma_{10}P_{\mathrm{r}}(x,t) + \gamma_{\mathrm{ar}}P_{\mathrm{a0}}(x,t),\end{aligned} \tag{12}$$

where $P_a(x,t)$ and $P_r(x,t)$ denote the distributions of anterogradely and retrogradely moving neurofilaments and $P_{a0}(x,t)$ and $P_{r0}(x,t)$ denote the distributions of anterogradely and retrogradely pausing neurofilaments. As shown above for the simpler two-state model, the spatial distribution of all neurofilaments in this model regardless of their kinetic state, i.e. $P(x,t) = P_a(x,t)+P_r(x,t)+P_{a0}(x,t)+P_{r0}(x,t)$, also approaches the Gaussian distribution shown in equation (10) (see appendix A). In appendices B and C, we show that the mean value $\langle x(t)\rangle$ and variance $\sigma^2(t)$ of the Gaussian distributions generated by this four-state model are given by

$$\frac{\mathrm{d}}{\mathrm{d}t}\langle x(t)\rangle \equiv \bar{v} = \frac{1}{(1+q_1)\gamma_{\mathrm{rev}}}(\gamma_{\mathrm{ra}}v_a + \gamma_{\mathrm{ar}}v_r) = \frac{1}{(1+q_1)(1+q_3)}(q_3 v_a + v_r) \tag{13}$$

$$\frac{\mathrm{d}}{\mathrm{d}t}\sigma^2(t) = \frac{2q_1}{\gamma_{01}+\gamma_{10}}\bar{v}^2 + 2\frac{1}{q_1(\gamma_{01}+\gamma_{10})}\frac{\gamma_{\mathrm{ra}}\gamma_{\mathrm{ar}}}{\gamma_{\mathrm{rev}}^2}\left(1+\frac{\gamma_{01}}{\gamma_{\mathrm{rev}}}\right)(v_a - v_r)^2, \tag{14}$$

with $\gamma_{\mathrm{rev}} \equiv \gamma_{\mathrm{ar}} + \gamma_{\mathrm{ra}}$ and $q_3 = \gamma_{\mathrm{ra}}/\gamma_{\mathrm{ar}}$. Note that the average velocity $\bar{v}$ depends only on the *ratios* of the transition rates $q_1 = \gamma_{10}/\gamma_{01}$ and the *ratios* of the reversal rates $q_3 = \gamma_{\mathrm{ra}}/\gamma_{\mathrm{ar}}$.

Experimental measurements are available for the transition rates $\gamma_{01}$ and $\gamma_{10}$ (equation (4)), but this is not the case for the reversal rates $\gamma_{\mathrm{ra}}$ and $\gamma_{\mathrm{ar}}$ because reversals are rare [7, 9, 10]. However, we do have information on the fraction of anterogradely and retrogradely moving neurofilaments, $f_a$ and $f_r$, and we can express these fractions in terms of the reversal rate constants as $f_a = \gamma_{\mathrm{ra}}/\gamma_{\mathrm{rev}}$ and $f_r = \gamma_{\mathrm{ar}}/\gamma_{\mathrm{rev}}$. Thus, $f_a/f_r = \gamma_{\mathrm{ra}}/\gamma_{\mathrm{ar}}$. For the rat and mouse superior cervical ganglion neuron data sets summarized in table 1, $f_a/f_r = \gamma_{\mathrm{ra}}/\gamma_{\mathrm{ar}} = 2.23$ and 0.89, respectively. Assuming an overall reversal frequency $\gamma_{\mathrm{rev}} = 1\times10^{-4}\ \mathrm{s}^{-1}$ [10], we obtain a rough estimate for the reversal rates of $\gamma_{\mathrm{ra}} \approx 6.9\times10^{-5}\ \mathrm{s}^{-1}$ and $\gamma_{\mathrm{ar}} \approx 3.1\times10^{-5}\ \mathrm{s}^{-1}$ for the rat superior cervical ganglion neuron data set, whereas for the mouse superior cervical ganglion neuron data set we obtain $\gamma_{\mathrm{ra}} \approx 4.7\times10^{-5}\ \mathrm{s}^{-1}$ and $\gamma_{\mathrm{ar}} \approx 5.3\times10^{-5}\ \mathrm{s}^{-1}$. However, it is important to emphasize that these are rough estimates because the number of reversals observed in our experimental studies is very small.

### 3.4. On-track and off-track states

To account for the existence of distinct prolonged pausing states, we now expand our model to include distinct on-track and off-track pausing states, both anterograde and retrograde. Neurofilaments in the on-track state alternate between bouts of rapid movement and short pauses, as described by the four-state model above, whereas neurofilaments in the off-track state pause for prolonged periods without movement [11]. A kinetic scheme for this extended model is shown in figure 4. According to this scheme, a neurofilament pausing on track in the anterograde or retrograde states has four possible fates within the time interval $\delta t$: (1) switch to the running state with rate $\gamma_{01}$, (2) switch off-track with rate $\gamma_{\mathrm{off}}$, (3) reverse direction with rates $\gamma_{\mathrm{ar}}$ or $\gamma_{\mathrm{ra}}$ or (4) remain in the on-track pausing state with probability $p_{00}$. Once a neurofilament is in the off-track state, it can switch back to the on-track state with rate $\gamma_{\mathrm{on}}$. To describe the behavior of an ensemble of neurofilaments according to this model, we use the following set of equations:

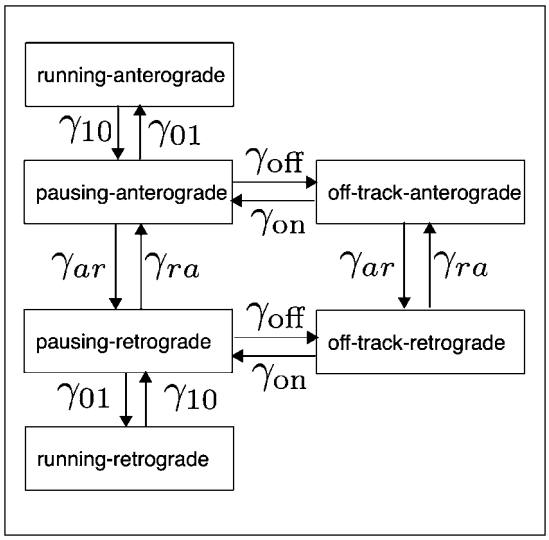


**Figure 4.** The kinetic scheme of neurofilament transport for a six-state model in which the filaments can enter an additional off-track pausing state in which they may pause for more extended periods.

$$\begin{aligned}
\frac{\partial P_a}{\partial t} &= -v_a\frac{\partial P_a}{\partial x} - \gamma_{10}P_a + \gamma_{01}P_{a0}\\
\frac{\partial P_r}{\partial t} &= -v_r\frac{\partial P_r}{\partial x} - \gamma_{10}P_r + \gamma_{01}P_{r0}\\
\frac{\partial P_{a0}}{\partial t} &= -(\gamma_{01}+\gamma_{ar})P_{a0} + \gamma_{10}P_a + \gamma_{ra}P_{r0} + \gamma_{on}P_{ap} - \gamma_{off}P_{a0}\\
\frac{\partial P_{r0}}{\partial t} &= -(\gamma_{01}+\gamma_{ra})P_{r0} + \gamma_{10}P_r + \gamma_{ar}P_{a0} + \gamma_{on}P_{rp} - \gamma_{off}P_{r0}\\
\frac{\partial P_{ap}}{\partial t} &= \gamma_{off}P_{a0} - \gamma_{on}P_{ap} - \gamma_{ar}P_{ap} + \gamma_{ra}P_{rp}\\
\frac{\partial P_{rp}}{\partial t} &= \gamma_{off}P_{r0} - \gamma_{on}P_{rp} - \gamma_{ra}P_{rp} + \gamma_{ar}P_{ap},
\end{aligned} \tag{15}$$

where $P_{ap}(x,t)$ and $P_{rp}(x,t)$ denote the distributions of off-track neurofilaments in the anterograde and retrograde states, respectively. As shown above for the simpler two-state and four-state models, the spatial distribution of all neurofilaments without regard to their kinetic state, i.e. $P(x,t) = P_a(x,t) + P_r(x,t) + P_{a0}(x,t) + P_{r0}(x,t) + P_{ap}(x,t) + P_{rp}(x,t)$, also approaches the Gaussian distribution shown in equation (10) (see appendix A). In appendices B and C, we show that the mean value $\langle x(t)\rangle$ and variance $\sigma^2(t)$ of the Gaussian distributions generated by this six-state model are given

by

$$\bar{v} = \frac{\mathrm{d}}{\mathrm{d}t}\langle x(t)\rangle = \frac{1}{\gamma_{\mathrm{rev}}}\frac{1}{1+q_1(1+q_2)}\left(\gamma_{\mathrm{ra}}v_{\mathrm{a}}+\gamma_{\mathrm{ar}}v_{\mathrm{r}}\right)$$
$$= \frac{1}{(1+q_1(1+q_2))\,(1+q_3)}\left(q_3 v_{\mathrm{a}}+v_{\mathrm{r}}\right) \qquad (16)$$

$$\frac{\mathrm{d}}{\mathrm{d}t}\sigma^2(t) = \frac{2\bar{v}^2 q_1}{1+q_1(1+q_2)}\left(\frac{q_2}{\gamma_{\mathrm{on}}}+\frac{(1+q_2)^2}{\gamma_{01}}\right)$$
$$+\frac{2\gamma_{\mathrm{ar}}\gamma_{\mathrm{ra}}}{\gamma_{\mathrm{rev}}^2}\frac{1}{\gamma_{10}}\frac{1}{1+q_1(1+q_2)}$$
$$\times\left(1+\frac{\gamma_{01}}{\gamma_{\mathrm{rev}}}\frac{\gamma_{\mathrm{on}}+\gamma_{\mathrm{rev}}}{\gamma_{\mathrm{on}}+\gamma_{\mathrm{off}}+\gamma_{\mathrm{rev}}}\right)(v_{\mathrm{a}}-v_{\mathrm{r}})^2\,, \qquad (17)$$

with $q_1 = \gamma_{10}/\gamma_{01}$ and $q_2 = \gamma_{\mathrm{off}}/\gamma_{\mathrm{on}}$.

Note that in these expressions, the average velocity of movement $\bar{v}$ depends only on the *ratios* of the kinetic rates $q_1 = \gamma_{10}/\gamma_{01}$, $q_2 = \gamma_{\mathrm{off}}/\gamma_{\mathrm{on}}$ and $q_3 = \gamma_{\mathrm{ra}}/\gamma_{\mathrm{ar}}$ in the following manner.

(a) For increasing values of the ratios $q_1 = \gamma_{10}/\gamma_{01}$ and $q_2 = \gamma_{\mathrm{off}}/\gamma_{\mathrm{on}}$, the average rate of movement slows down.
(b) For increasing values of the ratio $q_3 = \gamma_{\mathrm{ra}}/\gamma_{\mathrm{ar}}$, the average rate approaches that which it would have if it only moved anterograde without reversals.
(c) For decreasing values of the ratio $q_3 = \gamma_{\mathrm{ra}}/\gamma_{\mathrm{ar}}$, the average rate approaches that which it would have if the neurofilaments moved only retrogradely without reversals.

The rates $\gamma_{\mathrm{on}}$ and $\gamma_{\mathrm{off}}$ have been determined experimentally in cultured rat superior cervical ganglion neurons using a fluorescence photoactivation pulse-escape technique [11] and are $\gamma_{\mathrm{on}} = 2.75\times10^{-4}\ \mathrm{s}^{-1}$ and $\gamma_{\mathrm{off}} = 4.45\times10^{-3}\ \mathrm{s}^{-1}$. Knowing $\gamma_{10}$ and $\gamma_{01}$ (equation (5)) and the ratio $f_{\mathrm{a}}/f_{\mathrm{r}} = \gamma_{\mathrm{ra}}/\gamma_{\mathrm{ar}}$, we thus obtain an average velocity of $\bar{v} = 0.40$ mm/day for the rat superior cervical ganglion neuron data set.

In contrast to the average velocity, the spread of the Gaussian wave, $\sigma^2(t)$, depends on the kinetic rates *individually* in the following manner:

(a) For decreasing reversal rates $\gamma_{\mathrm{ar}}$ and/or $\gamma_{\mathrm{ra}}$, the rate of spreading *increases* because when reversals are less frequent, the duration of the bouts of anterograde and retrograde movements between reversals increases.
(b) For a fixed rate $\gamma_{\mathrm{off}}$ and decreasing rates $\gamma_{\mathrm{on}}$, the rate of spreading *decreases* because each neurofilament spends more time off track and hence less time moving. For the same reason, the average velocity is also slower. This fact will be of significance for the data interpretation below (see section 5).
(c) For a fixed rate $\gamma_{\mathrm{on}}$ and decreasing rates $\gamma_{\mathrm{off}}$, the rate of spreading *increases* because the neurofilaments spend more time on track and hence more time moving.

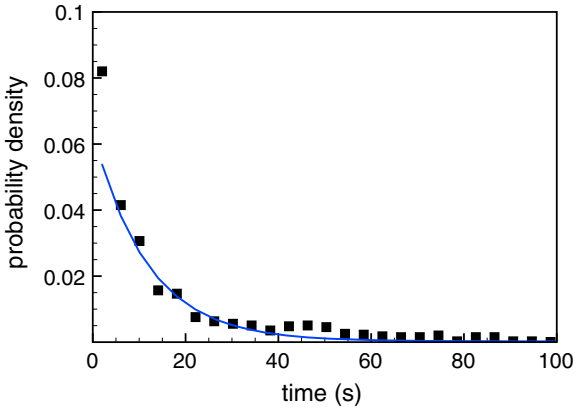


**Figure 5.** Probability density distribution of pause durations (symbols) extracted directly from our experimental data on neurofilament movement in cultured neurons from mouse superior cervical ganglia, compared with those predicted by the six-state model. The predicted distribution (line) was obtained using the expression $\gamma_{01}\exp(-\gamma_{01}t)$, which is valid for short times (see text). The transition rate $\gamma_{01}$ for the mouse superior cervical ganglion neuron data set is given by equation (6).

## 4. Pause-time distribution

An important characteristic of the stop-and-go movement of neurofilaments is the frequency distribution of the pause durations. For our six-state model, which includes distinct on-track and off-track pausing states, we expect many brief on-track pauses and fewer prolonged off-track pauses. This results in a biphasic distribution of pause durations [13]. Due to the short duration of our time-lapse movies, we are not able to observe long pauses in our live-cell imaging observations on neurofilaments moving through gaps. However, the pause duration distribution obtained from these data should be reproduced by our model for short durations (up to about a minute) [13]. In appendix D, we derive the exact expression for the distribution of pause durations based on the six-state kinetic model described in the previous section, i.e.

$$\rho(t) = \left(\frac{\gamma_{01}+\lambda_-}{\lambda_+-\lambda_-}\right)\lambda_+\exp(\lambda_+ t)$$
$$-\left(1+\frac{\gamma_{01}+\lambda_-}{\lambda_+-\lambda_-}\right)\lambda_-\exp(\lambda_- t)\,, \qquad (18)$$

with

$$\lambda_\pm = -\tfrac{1}{2}(\gamma_{01}+\gamma_{\mathrm{on}}+\gamma_{\mathrm{off}})$$
$$\pm\tfrac{1}{2}\sqrt{(\gamma_{01}+\gamma_{\mathrm{on}}+\gamma_{\mathrm{off}})^2-4\gamma_{01}\gamma_{\mathrm{on}}}. \qquad (19)$$

On short timescales the second term in equation (18) predominates, giving rise to a distribution that is approximately the simple exponential decay $\gamma_{01}\exp(-\gamma_{01}t)$. In figure 5, we use this approximation to compare the pause duration distribution extracted directly from our experimental observations on neurofilament movement in mouse superior cervical ganglion neurons with our model (appendix D). There is good agreement between the theoretical and experimental curves, which both exhibit exponential decay. For longer times, which are not available from the experimental data, the

theory predicts a transition to a slower exponential decay with time constant $1/\lambda_{on}$ (not shown in figure 5).

The average pause duration $\langle T \rangle$ predicted by the model can be obtained from equation (18), i.e.

$$\langle T \rangle = \int_0^\infty t\rho(t)\,\mathrm{d}t = -\frac{1}{\lambda_-} - \frac{\gamma_{01} + \lambda_-}{\lambda_-\lambda_+}. \tag{20}$$

This expression yields average pause durations of 414 s and 269 s for the rat and mouse superior cervical ganglion neuron data sets, respectively.

The pause duration distribution for off-track pauses (excluding on-track pauses; see equation (D.15)), i.e.

$$\rho_{off}(t) = \gamma_{on}\,\mathrm{e}^{-\gamma_{on}t}, \tag{21}$$

yields the following expression for the average off-track pause duration:

$$\langle T_{off} \rangle = \int_0^\infty t\rho_{off}(t)\,\mathrm{d}t = \frac{1}{\gamma_{on}}. \tag{22}$$

The pause duration distribution for on-track pauses (excluding off-track pauses; see equation (D.17)), i.e.

$$\rho_{on} = (\gamma_{off} + \gamma_{01})\exp(-(\gamma_{off} + \gamma_{01})t), \tag{23}$$

yields the following expression for the average on-track pause duration:

$$\langle T_{on} \rangle = \int_0^\infty t\rho_{on}(t)\,\mathrm{d}t = \frac{1}{\gamma_{off} + \gamma_{01}}. \tag{24}$$

The expressions in equations (22) and (24) yield an average off-track pause duration of $\langle T_{off} \rangle = 60.5$ min and an average on-track pause duration of $\langle T_{on} \rangle = 21.8$ s for the rat superior cervical ganglion neuron data set. These on-track and off-track average pause durations are broadly consistent with our estimates of $\langle T_{off} \rangle = 61$ min and $\langle T_{on} \rangle = 29$ s in rat superior cervical ganglion neurons using a discrete stochastic modeling approach [11].

## 5. Slow axonal transport in the mouse sciatic nerve

In the previous sections, we derived expressions that relate the movement of a population of neurofilaments in axons to the moving and pausing behavior of the individual neurofilaments. These expressions should allow us to extract information about the fast timescale behavior of neurofilaments from pulse-labeling kinetics obtained on slow timescales and to predict the pulse-labeling kinetics based on the fast timescale behavior. To test this, we now use our model to analyze the radioisotopic pulse labeling data of Xu and Tung [17, 25] for neurofilament protein L in adult mouse spinal motor neurons (figure 6). These data were obtained by injecting radioactive amino acid (35S-methionine) into the vicinity of motor neuron cell bodies in the anterior horn of the mouse spinal cord at level L5. This results in a pulse of radiolabeled proteins in motor axons which enter the sciatic nerve via the L5 ventral nerve root. As predicted by our model (see appendix A), the pulse of radiolabeled proteins forms a Gaussian wave which decreases in height and increases in width as it propagates along the nerve.

To analyze the velocity and spreading of the Gaussian transport waves in mouse spinal motor neurons, we determined the mean and variance of the distributions at each time point in figure 6 and plotted these values versus time. As noted by Xu and Tung [17, 25], the best fit through the mean values is given by two line segments, which intersect at about 3–4 weeks (figure 7). The slope of the first line, which is the average transport velocity for weeks 1–3, is 0.6 mm/day. This is similar to the value of 0.56 mm/day determined in our prior study using stochastic simulations [13]. In contrast, the slope of the second line, which is the average velocity for weeks 4–6, is 0.12 mm/day. Thus there appears to be a five-fold slowing of neurofilament transport along these nerves at about 3–4 weeks after injection, when the peak of the transport wave is about 14 mm from the spinal cord.

Interestingly, however, our analysis also shows that the *decrease* in the velocity of the Gaussian wave coincides approximately with a 2.5-fold *increase* in the variance, from 1.3 $\mathrm{mm}^2$/day in weeks 1–3 to 3.3 $\mathrm{mm}^2$/day in weeks 4–6 (figure 7(b)). To explain these kinetic changes in terms of our model, we use equations (16) and (17) derived above, which express the velocity and the rate of spreading of the Gaussian transport wave in terms of the rate constants in our model. We use the transition rates $\gamma_{01} = 6.4 \times 10^{-2}\ \mathrm{s}^{-1}$ and $\gamma_{10} = 0.14\ \mathrm{s}^{-1}$, obtained by tracking neurofilaments in cultured mouse superior cervical ganglion neurons (equation (6)), and we use the on- and off-track rates $\gamma_{on} = 2.8 \times 10^{-4}\ \mathrm{s}^{-1}$ and $\gamma_{off} = 4.5 \times 10^{-3}\ \mathrm{s}^{-1}$, obtained using the fluorescence photoactivation pulse-escape method in cultured rat superior cervical ganglion neurons [11]. As explained above, we do not have a reliable estimate for the reversal rates in cultured neurons because reversals are relatively rare. However, since we know that the velocity $\bar{v}$ depends on the ratio $\gamma_{ra}/\gamma_{ar}$, we can solve equation (16) for weeks 1–3 to obtain $\gamma_{ra}/\gamma_{ar} = 3.4$. Knowing this ratio and the rate of spreading in weeks 1–3 (see above), we can solve equation (17) to obtain the individual rates $\gamma_{ra} = 1.4 \times 10^{-5}\ \mathrm{s}^{-1}$ and $\gamma_{ar} = 4.2 \times 10^{-6}\ \mathrm{s}^{-1}$. These values are within an order of magnitude of the rough estimates that we made based on the few reversals that we have observed experimentally (see above).

Next, we ask what changes in the kinetic parameters of our model could explain the slower velocity and increased rate of spreading of the transport wave in weeks 4–6. One way to decrease the average velocity is to decrease the speed of anterograde movement, $v_a$. However, this cannot explain the experimental data because it leads to a simultaneous decrease in the rate of spreading. Another way to decrease the average velocity is to increase the speed of retrograde movement, $v_r$. Using equation (16) for the average velocity, we find that we have to increase $v_r$ by about 300% to $-1.45\ \mu\mathrm{m\,s}^{-1}$ in order to match the observed slowing of the neurofilament transport wave in the experimental data. This far exceeds the average velocities observed for neurofilaments in cultured neurons. Moreover, while this increase does also result in a simultaneous increase in the rate of spreading, the extent of this increase is 40% greater than observed experimentally. Thus, it seems very unlikely that an increase in the speed of retrograde movement can explain the experimental data.

In our model, there are two other ways to explain the slower velocity and increased rate of spreading of the transport

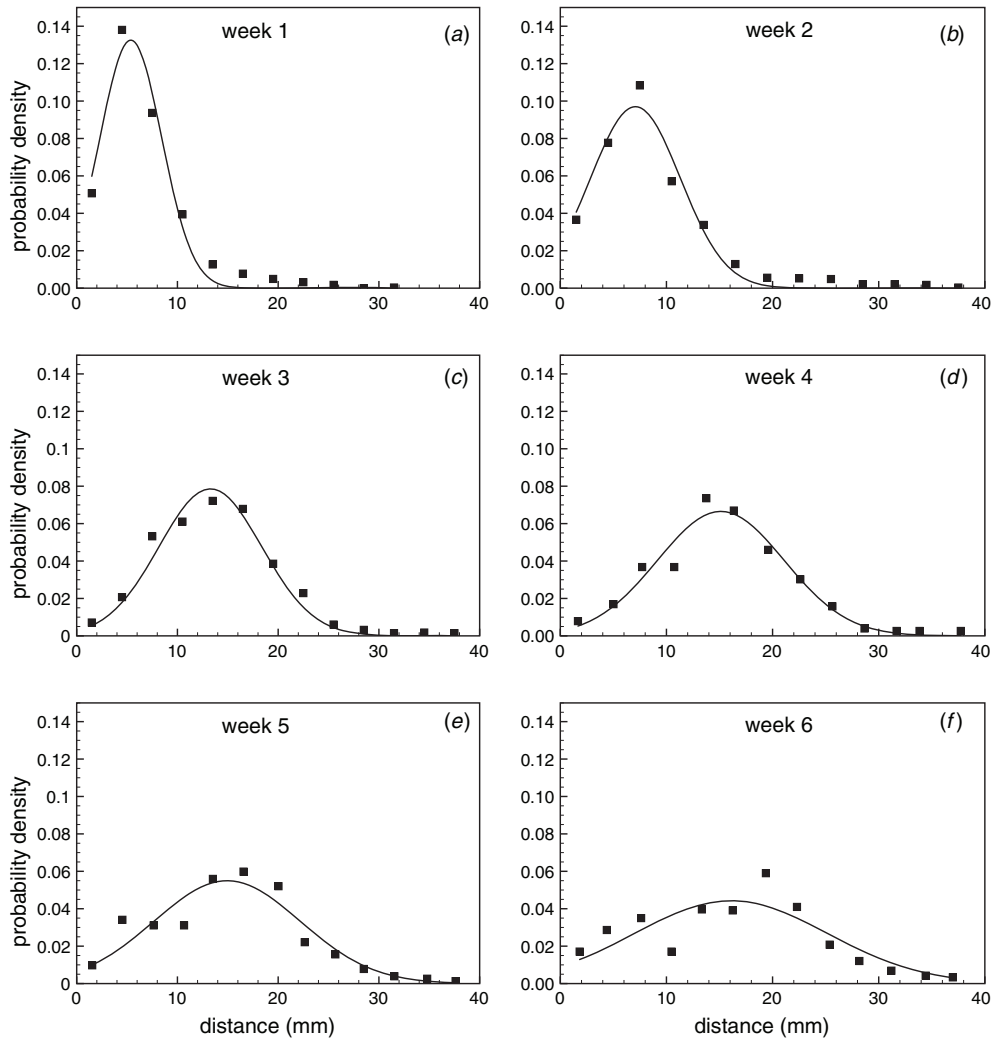


**Figure 6.** Transport of a pulse of radiolabeled neurofilaments along adult mouse spinal motor axons. Each graph depicts the distribution of radioactive neurofilament protein L along the ventral root and sciatic nerve at one of six injection-sacrifice intervals, ranging from 1 to 6 weeks (*a*)–(*f*), respectively. The *x*-axis represents distance measured within the measurement window, which extended 39 mm from the point that the axons exit the spinal cord. The *y*-axis represents the probability density of the distribution. Each data point (symbols) corresponds to the amount of radioactive neurofilament protein L in one 3 mm segment of nerve (average of 3–5 nerves). In the original study of Xu and Tung [25] from which these data were obtained, the profiles were normalized to the total radioactivity within the measurement window. However, this is problematic because the measurement window does not include the entire wave at every time point, particularly at early times when the radiolabeled proteins are still entering the window. To deal with this, we fitted the data points at each time point with a Gaussian curve (line), multiplied this Gaussian distribution by a factor that yields an integral under the curve of 1 and then normalized the data points to the total area under this Gaussian including the portions that extended beyond the measurement window. Thus, the experimental profiles represent neurofilament probability density distributions with a conserved normalization, permitting direct comparison of the shape and height of the waves at different time points. This approach assumes that the neurofilaments are very long-lived (i.e. there is negligible loss of protein due to degradation), which is supported by recent measurements of the half-life of neurofilaments *in vivo* [26]. Data from [25].

wave in weeks 4–6. One is to increase the number of retrogradely moving filaments by increasing $\gamma_{ar}$ or decreasing $\gamma_{ra}$, and the other is to decrease the proportion of the time that the filaments spend on track by decreasing $\gamma_{on}$ or increasing $\gamma_{off}$. An important observation guiding this process is that the rate of movement is given by the difference of two velocity terms in the numerator $\gamma_{ra} v_a$, which is positive, and $\gamma_{ar} v_r$, which is negative; see equation (16). Hence, the rate of movement can be zero without a single term having to be zero, which suggests that the velocity is more sensitive to changes in the reversal rate constants than to changes in the other rate constants ($q_1$ and $q_2$), which are confined to the denominator.

First, we examine alterations in the reversal rate constants, which determine the directionality of neurofilament movement. To adjust the rate of movement from 0.6 mm/ day to 0.12 mm/day, we decrease the ratio $\gamma_{ra}/\gamma_{ar}$ from 3.4 to 1.3. Knowing this ratio and the rate of spreading in weeks 4–6 (see above), we can solve equation (17) to obtain the reversal rates. We find that the rate $\gamma_{ar}$ *remains unchanged*, i.e. $\gamma_{ar} = 4.2 \times 10^{-6}\ s^{-1}$ whereas $\gamma_{ra}$ decreases by about a factor of 2.5 to $\gamma_{ra} = 5.4 \times 10^{-6}\ s^{-1}$. This corresponds to a decrease in the proportion of the time that the filaments spend moving anterogradely, which is given by $\gamma_{ra}/(\gamma_{ar} + \gamma_{ra})$, from 77% in weeks 1–3 to 56% in weeks 3–4. These proportions are within

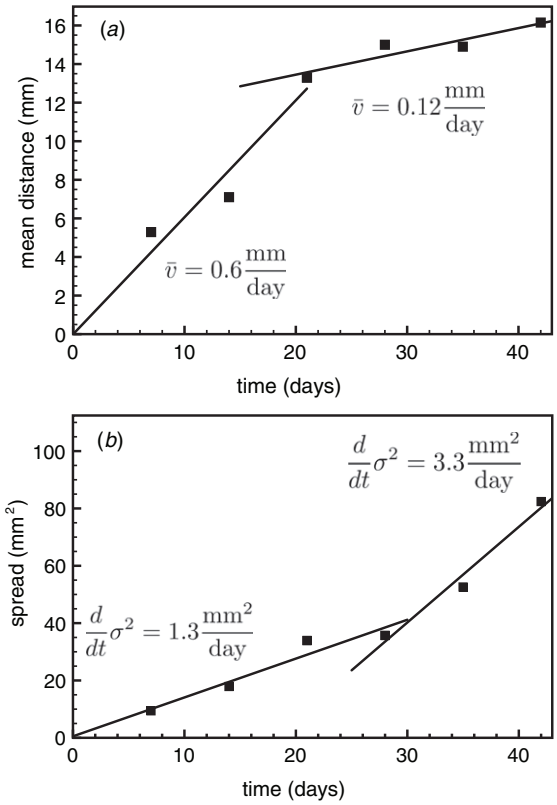


**Figure 7.** Velocity and spreading of the Gaussian transport wave in mouse spinal motor neurons as a function of time, based on the data in figure 6. The $y$-axis in ($a$) shows the mean distance from the spinal cord traveled by the pulse of radiolabeled neurofilaments. The $y$-axis in ($b$) shows the variance of the Gaussian transport wave, which is a measure of its width. The lines represent linear curve fits for weeks 1–3 and 4–6.

the range (47–83% anterograde) that we have encountered in our live-cell imaging studies on cultured neurons [7, 9, 10] (see also table 1). Remarkably, both the slower velocity *and* the increased rate of spreading of the transport wave can be explained by the decrease of *one single kinetic rate*, the reversal rate $\gamma_{\text{ra}}$.

Finally, we examine alterations in the on- and off-track rate constants, which determine the proportion of the time that the filaments spend engaged with their microtubule tracks. Of great importance here is that in order to slow down the rate of movement, the prefactor in equations (16) and (17), which is a function of $\gamma_{\text{off}}/\gamma_{\text{on}}$, has to decrease. To adjust the rate of movement from 0.6 mm/day to 0.12 mm/day we increase the ratio $\gamma_{\text{off}}/\gamma_{\text{on}}$ from 16.2 to 87, which is a change of about a factor of 5. We then solve equation (17) for the individual rates $\gamma_{\text{on}}$ and $\gamma_{\text{off}}$ as described above. To match the rate of spreading in weeks 4–6, we find that the on- and off-track rate constants have to be reduced by more than two orders of magnitude to $\gamma_{\text{on}} = 7.8 \times 10^{-7}\ \text{s}^{-1}$ and $\gamma_{\text{off}} = 6.8 \times 10^{-5}\ \text{s}^{-1}$ respectively. In other words, $\gamma_{\text{on}}$ and $\gamma_{\text{off}}$ would have to be reduced by more than a factor of 100 compared to our experimental measurements in cultured neurons [11]. While it is formally possible that the on- and off-track rates could differ by this much *in vivo*, the greater sensitivity of the velocity and spreading to the reversal rate constants discussed above makes it more likely that changes in the reversal rates (i.e. the balance of anterograde and retrograde movements) underlie the kinetic transition at weeks 3–4 in these neurons.

## 6. Discussion and conclusions

We have previously described a stochastic model of neurofilament transport *in vivo* based on direct measurements of neurofilament movement in cultured neurons [13]. This model assumed multiple velocity states and was only accessible through computational simulations. In the present study, we developed a simpler model with only three velocity states that is more amenable to analytical approaches. Using this model, we have shown rigorously that a pulse of radiolabeled neurofilaments approaches a Gaussian waveform as it moves out along the axon, similar to that observed in the experimental data. Since a Gaussian wave can be fully described by just two cumulants, the mean and the standard deviation, this means that the same also applies to the neurofilament transport waves obtained in radioisotopic pulse-labeling experiments. To analyze the kinetics of neurofilament transport, we derived explicit expressions for these cumulants in terms of the rate constants in our model. The power of these expressions is that they permit us to calculate the velocity and rate of spreading of a population of radiolabeled neurofilaments based on the transport kinetics of single neurofilament polymers and conversely to extract the transport kinetics of single neurofilament polymers from the velocity and rate of spreading of the neurofilament transport waves.

To explore the utility of this analytical approach, we investigated the possible causes of the slowing of neurofilament transport along axons, which is a poorly understood phenomenon. We selected the published radioisotopic pulse-labeling data of Xu and Tung [17] for neurofilament protein L in mouse spinal motor neurons. These data reveal an abrupt slowing of neurofilament transport at approximately 3–4 weeks after injection when the peak of the neurofilament wave is about 14 mm from the spinal cord. This differs from the more gradual slowing reported in rat spinal motor neurons [14–16], but it is a good data set for our modeling study because the standard errors of the data are small and the kinetics are relatively clean. Approximately coincident with the decrease in velocity, which was noted by Xu and Tung [17], we also observed an increase in the rate of spreading. Using our model, we found that the decrease in the velocity and the increase in the rate of spreading can both be explained by the decrease of a single kinetic rate, the reversal rate $\gamma_{\text{ra}}$, by a factor of about 2.5, while all other kinetic rates remain constant. The effect of this change is to decrease the frequency with which neurofilaments switch from retrograde to anterograde movement, thereby increasing the relative proportion of the time that neurofilaments spend moving retrogradely. We were also able to reproduce the observed changes in velocity and spreading by changing the on- and off-track rates, but only if we changed them by two orders of magnitude. Thus the velocity and spreading of the neurofilament transport wave are particularly sensitive to changes in the reversal rate constants, which determine the

frequency of reversals and the balance of anterograde and retrograde movements. Based on this finding, we propose that changes in the reversal frequency are the most likely explanation for the slowing of neurofilament transport in mouse spinal motor neurons. At this point we have made no attempt to predict whether such changes are due to temporal factors (development or aging) or to spatial factors (inhomogeneities along the axon), but this will be an interesting topic for future investigation.

To understand how changes in a reversal rate constant might regulate neurofilament transport in axons, it will be necessary to understand the molecular mechanism of neurofilament movement. Several lines of evidence indicate that neurofilaments are transported along microtubule tracks powered by microtubule motor proteins [27–32]. The anterograde motor appears to be kinesin-1 and the retrograde motor appears to be dynein. However, the mechanism by which neurofilaments and other intracellular cargoes switch from one direction of movement to the other is not known. Three models are generally considered [33]. According to the tug-of-war model, individual cargoes can simultaneously bind both anterograde and retrograde motors, and the direction of movement is determined by a competition between these opposing motors. Alternatively, according to the exclusionary presence model, individual cargoes can bind only motors of a single directionality at one time. Finally, according to the coordination model, each cargo is bound to both anterograde and retrograde motors but the activity of these motors is coordinated, either physically or mechanically, to determine the direction of movement. Thus the slowing of neurofilament transport analyzed in the present study could theoretically be explained by an increase in the number, affinity and/or activity of retrograde motors bound to the moving neurofilaments. It is not known which of these possible mechanisms actually occur, but studies on the bidirectional transport of vesicular cargoes tend to favor a coordination model in which anterograde and retrograde motors form a dual motor complex that is regulated by a putative molecular switch [34, 35].

The best understood role of neurofilaments in axons is as space-filling structures that maximize axonal caliber [36, 37]. This is important because the rate of propagation of action potentials is directly proportional to the axonal cross-sectional area. Thus, it is important to understand the mechanisms that regulate the neurofilament content of axons. The intermittent and bidirectional motile behavior of neurofilaments in axons suggests that one important determinant may be the balance of anterograde and retrograde movements and pauses. For example, if neurofilaments pause more, or if those that move spend more of their time moving retrogradely, their residence time in the axon will increase and they will tend to accumulate, resulting in an increase in axon caliber. In this way, the transport properties of neurofilaments may directly influence axonal morphology and physiology. Similarly, it is attractive to speculate that perturbations in the directionality and/or pausing behavior of neurofilaments may also give rise to the abnormal and sometimes massive accumulations of axonal neurofilaments that are observed in many neurodegenerative diseases.

The problem of how neurofilaments are transported in axons is particularly well suited to mathematical modeling because it is not presently possible to analyze the movement of single neurofilaments on both fast and slow timescales in the same experimental system. Thus our model provides a tool for reconciling the kinetic data obtained by direct observation of single neurofilaments in cultured nerve cells, on a timescale of seconds or minutes, with the kinetics data obtained for populations of neurofilaments *in vivo* by radioisotopic pulse labeling, on a timescale of days or weeks. Importantly, our model is based on kinetic parameters that are measurable experimentally. In this way, our model makes minimal assumptions about the molecular mechanism and regulation of neurofilament transport, which are still largely unknown. Though such a modeling approach is phenomenological, the present study demonstrates that it can provide insights into the transport mechanism that cannot be obtained by experimentation alone.

## Acknowledgments

We thank the National Science Foundation for financial support under grants IOS-0818412 (PJ) and IOS-0818653 (AB).

## Appendix A. The transport waves are Gaussian

Here we show that the spatial distribution of a pulse of radio-labeled neurofilaments in our six-state model (equation (15)) approaches a Gaussian distribution and is hence fully characterized by the mean value and the variance. The same arguments also apply to the two-state and four-state models in equations (7) and (12), respectively.

We start by showing that all cumulants of the distribution of neurofilaments $P(x,t)$ are linear in time. To this end, we introduce the Fourier transforms $\phi_{\mathrm{a,r,a0,r0,ap,rp}}(k,t)$ of the distributions $P_{\mathrm{a,r,a0,r0,ap,rp}}(x,t)$ and obtain their equations of motion

$$\begin{aligned}
\frac{\partial\phi_{\mathrm{a}}(k,t)}{\partial t} &= v_{\mathrm{a}}k\phi_{\mathrm{a}} - \gamma_{10}\phi_{\mathrm{a}} + \gamma_{01}\phi_{\mathrm{a0}}\\
\frac{\partial\phi_{\mathrm{r}}(k,t)}{\partial t} &= v_{\mathrm{r}}k\phi_{\mathrm{r}} - \gamma_{10}\phi_{\mathrm{r}} + \gamma_{01}\phi_{\mathrm{r0}}\\
\frac{\partial\phi_{\mathrm{a0}}(k,t)}{\partial t} &= -(\gamma_{01}+\gamma_{\mathrm{ar}})\phi_{\mathrm{a0}} + \gamma_{10}\phi_{\mathrm{a}} + \gamma_{\mathrm{ra}}\phi_{\mathrm{r0}} + \gamma_{\mathrm{on}}\phi_{\mathrm{ap}} - \gamma_{\mathrm{off}}\phi_{\mathrm{a0}}\\
\frac{\partial\phi_{\mathrm{r0}}(k,t)}{\partial t} &= -(\gamma_{01}+\gamma_{\mathrm{ra}})\phi_{\mathrm{r0}} + \gamma_{10}\phi_{\mathrm{r}} + \gamma_{\mathrm{ar}}\phi_{\mathrm{a0}} + \gamma_{\mathrm{on}}\phi_{\mathrm{rp}} - \gamma_{\mathrm{off}}\phi_{\mathrm{r0}}\\
\frac{\partial\phi_{\mathrm{ap}}(k,t)}{\partial t} &= \gamma_{\mathrm{off}}\phi_{\mathrm{a0}} - \gamma_{\mathrm{on}}\phi_{\mathrm{ap}} - \gamma_{\mathrm{ar}}\phi_{\mathrm{ap}} + \gamma_{\mathrm{ra}}\phi_{\mathrm{rp}}\\
\frac{\partial\phi_{\mathrm{rp}}(k,t)}{\partial t} &= \gamma_{\mathrm{off}}\phi_{\mathrm{r0}} - \gamma_{\mathrm{on}}\phi_{\mathrm{rp}} - \gamma_{\mathrm{ra}}\phi_{\mathrm{rp}} + \gamma_{\mathrm{ar}}\phi_{\mathrm{ap}}.
\end{aligned} \tag{A.1}$$

The characteristic function $\phi(k,t)$ is associated with the distribution of all neurofilaments $P(x,t) = P_{\mathrm{a}}(x,t) + P_{\mathrm{r}}(x,t) + P_{\mathrm{a0}}(x,t) + P_{\mathrm{r0}}(x,t) + P_{\mathrm{ap}}(x,t) + P_{\mathrm{rp}}(x,t)$, and thus we can write

$$\begin{aligned}
\phi(k,t) \equiv\ & \phi_{\mathrm{a}}(k,t) + \phi_{\mathrm{r}}(k,t) + \phi_{\mathrm{a0}}(k,t)\\
& + \phi_{\mathrm{r0}}(k,t) + \phi_{\mathrm{ap}}(k,t) + \phi_{\mathrm{rp}}(k,t).
\end{aligned} \tag{A.2}$$

Assuming that all neurofilaments start at the same location, say $x = 0$, the characteristic functions $\phi_i(k,t)$ assume the values $\hat{P}_i$, i.e. the fraction of neurofilaments which are initially in state '$i$', at time $t = 0$. This leads to solutions of the form

$$\phi_i(k,t) = \hat{P}_i \exp(\lambda(k)t), \tag{A.3}$$

and hence

$$\phi(k,t) = \underbrace{\sum_i \hat{P}_i}_{=1} \exp(\lambda(k)t) \equiv \exp(\chi(k,t)). \tag{A.4}$$

Inserting equation (A.4) into equations (A.1) yields a set of equations for the function $\lambda(k)$. The function $\chi(k,t)$ is also known as the *cumulant generating function* since the coefficients of the Taylor expansion of $\chi(k,t)$ in terms of $k$ are the cumulants $K_n$, i.e.

$$\chi(k,t) = \sum_{s=1}^{\infty} \frac{(-\mathrm{i}k)^s}{s!} K_s(t). \tag{A.5}$$

The cumulant generating function is a linear function in time, and hence all the cumulants $K_s$ are linear functions in time, i.e. $K_s(t) = C_s t$. It is possible to extract the mean value $K_1(t) = \langle x(t)\rangle \equiv \bar{v}t$ and the variance $K_2(t) = \langle x^2(t)\rangle - \langle x(t)\rangle^2 \equiv \sigma^2(t)$ from the set of linear equations obtained after inserting the Taylor expansion in equation (A.5) into equation (A.3), and then into equation (A.1), and comparing coefficients of equal powers in $k$. However, a less cumbersome method is presented in appendices B and C.

Given the cumulant generating function $\chi(k,t)$, we can reconstruct the probability density using the inverse Fourier transform, i.e.

$$\begin{aligned} P(x,t) &= \frac{1}{2\pi}\int_{-\infty}^{\infty} \exp(\mathrm{i}kx)\cdot\exp(\chi(k,t))\,\mathrm{d}k \\ &= \frac{1}{2\pi}\int_{-\infty}^{\infty} \exp\left(\mathrm{i}kx - \mathrm{i}kK_1 - \frac{1}{2}k^2K_2 \right. \\ &\quad \left. + \sum_{s=3}^{\infty}\frac{(-\mathrm{i}k)^s}{s!}K_s(t)\right)\mathrm{d}k. \end{aligned} \tag{A.6}$$

We now perform two operations to further analyze this expression. First, we perform a time-dependent shift $\tilde{x} \equiv x - \bar{v}t$ which allows us to combine the first two terms in the exponent of the integrand in equation (A.6) as $\mathrm{i}kx - \mathrm{i}kK_1 = \mathrm{i}k\tilde{x}$. Second, we introduce the scaled variable $\tilde{k} = kt^{1/2}$, leading to

$$\begin{aligned} P(\tilde{x},t) &= \frac{1}{2\pi\sqrt{t}}\int_{-\infty}^{\infty}\exp\left(\frac{\mathrm{i}\tilde{k}\tilde{x}}{\sqrt{t}} - \frac{1}{2}D\tilde{k}^2\right) \\ &\quad \times \exp\left(\sum_{s=3}^{\infty}\frac{(-\mathrm{i}\tilde{k})^s}{s!}K_s(t)t^{-s/2}\right)\mathrm{d}\tilde{k}. \end{aligned} \tag{A.7}$$

Since the cumulants $K_s(t)$ all increase linear in time, all terms under the sum in equation (A.7) vanish for long times, and what is left are the linear and quadratic terms in $\tilde{k}$ which can be integrated to yield the Gaussian distribution

$$P(x,t) \approx \frac{1}{\sqrt{2\pi Dt}}\exp\left(\frac{-(x-\bar{v}t)^2}{2Dt}\right), \tag{A.8}$$

with

$$D = \frac{K_2(t)}{t}. \tag{A.9}$$

## Appendix B. Derivation of an expression for the average velocities

Here we derive expressions for the average transport velocity of neurofilaments based on the six-state, four-state and two-state models. For the six-state model in equation (15), the average velocity is defined as

$$\begin{aligned} \langle x(t)\rangle = \int_{-\infty}^{\infty} x(&P_{\mathrm{a}}(x,t) + P_{\mathrm{r}}(x,t) + P_{\mathrm{a0}}(x,t) \\ &+ P_{\mathrm{r0}}(x,t) + P_{\mathrm{ap}}(x,t) + P_{\mathrm{ar}}(x,t))\,\mathrm{d}x. \end{aligned} \tag{B.1}$$

Taking the derivative with respect to time, carrying it under the integral and utilizing the equations of motion in equation (15) result in

$$\begin{aligned} \frac{\mathrm{d}}{\mathrm{d}t}\langle x(t)\rangle &= -v_{\mathrm{a}}\int_{-\infty}^{\infty} x\frac{\partial P_{\mathrm{a}}(x,t)}{\partial x}\,\mathrm{d}x \\ &\quad - v_{\mathrm{r}}\int_{-\infty}^{\infty} x\frac{\partial P_{\mathrm{r}}(x,t)}{\partial x}\,\mathrm{d}x, \end{aligned} \tag{B.2}$$

and after integration in parts

$$\frac{\mathrm{d}}{\mathrm{d}t}\langle x(t)\rangle = v_{\mathrm{a}}\hat{P}_{\mathrm{a}}(t) + v_{\mathrm{r}}\hat{P}(t)_{\mathrm{r}}, \tag{B.3}$$

where

$$\hat{P}_{\mathrm{a,r}}(t) = \int_{-\infty}^{\infty} P_{\mathrm{a,r}}(x,t)\,\mathrm{d}x \tag{B.4}$$

denotes the probability of finding a neurofilament anywhere along the axon moving anterogradely or retrogradely.

Next, integration of all equations in equation (15) yields a set of linear equations for the probability $\hat{P}_i$ of finding a neurofilament in each of the kinetic states '$i$', i.e.

$$\begin{aligned} \frac{\mathrm{d}}{\mathrm{d}t}\hat{P}_{\mathrm{a}} &= -\gamma_{10}\hat{P}_{\mathrm{a}} + \gamma_{01}\hat{P}_{\mathrm{a0}} \\ \frac{\mathrm{d}}{\mathrm{d}t}\hat{P}_{\mathrm{r}} &= -\gamma_{10}\hat{P}_{\mathrm{r}} + \gamma_{01}\hat{P}_{\mathrm{r0}} \\ \frac{\mathrm{d}}{\mathrm{d}t}\hat{P}_{\mathrm{a0}} &= -(\gamma_{01}+\gamma_{\mathrm{ar}}+\gamma_{\mathrm{off}})\hat{P}_{\mathrm{a0}} + \gamma_{10}\hat{P}_{\mathrm{a}} + \gamma_{\mathrm{ra}}\hat{P}_{\mathrm{r0}} + \gamma_{\mathrm{on}}\hat{P}_{\mathrm{ap}} \\ \frac{\mathrm{d}}{\mathrm{d}t}\hat{P}_{\mathrm{r0}} &= -(\gamma_{01}+\gamma_{\mathrm{ra}}+\gamma_{\mathrm{off}})\hat{P}_{\mathrm{r0}} + \gamma_{10}\hat{P}_{\mathrm{r}} + \gamma_{\mathrm{ar}}\hat{P}_{\mathrm{a0}} + \gamma_{\mathrm{on}}\hat{P}_{\mathrm{ap}} \\ \frac{\mathrm{d}}{\mathrm{d}t}\hat{P}_{\mathrm{ap}} &= \gamma_{\mathrm{off}}\hat{P}_{\mathrm{a0}} - (\gamma_{\mathrm{ar}}+\gamma_{\mathrm{on}})\hat{P}_{\mathrm{ap}} + \gamma_{\mathrm{ra}}\hat{P}_{\mathrm{rp}} \\ \frac{\mathrm{d}}{\mathrm{d}t}\hat{P}_{\mathrm{rp}} &= \gamma_{\mathrm{off}}\hat{P}_{\mathrm{r0}} - (\gamma_{\mathrm{ra}}+\gamma_{\mathrm{on}})\hat{P}_{\mathrm{rp}} + \gamma_{\mathrm{ar}}\hat{P}_{\mathrm{ap}}. \end{aligned} \tag{B.5}$$

Steady-state solutions are easily obtained, leading to

$$\begin{aligned} \hat{P}_{\mathrm{a}} &= \frac{\gamma_{\mathrm{ra}}}{\gamma_{\mathrm{rev}}}\frac{1}{1+q_1(1+q_2)} \\ \hat{P}_{\mathrm{r}} &= \frac{\gamma_{\mathrm{ar}}}{\gamma_{\mathrm{rev}}}\frac{1}{1+q_1(1+q_2)}, \end{aligned} \tag{B.6}$$

and hence

$$\bar{v} = \frac{1}{1+q_1(1+q_2)}\frac{1}{\gamma_{\mathrm{rev}}}(\gamma_{\mathrm{ra}}v_{\mathrm{a}} + \gamma_{\mathrm{ar}}v_{\mathrm{r}}). \tag{B.7}$$

For the four-state model in equation (12), which lacks off-track transitions (i.e. $\gamma_{\mathrm{on}} = \infty$, $\gamma_{\mathrm{off}} = 0$), this expression simplifies to

$$\bar{v} = \frac{1}{1+q_1}\frac{1}{\gamma_{\mathrm{rev}}}(\gamma_{\mathrm{ra}}v_{\mathrm{a}} + \gamma_{\mathrm{ar}}v_{\mathrm{r}}). \tag{B.8}$$

For the two-state model in equation (7), which lacks reversals and off-track transitions (i.e. $\gamma_{\rm off}=0$, $\gamma_{\rm ra}=\gamma_{\rm ar}=0$ and $v_{\rm a}=v_{\rm r}\equiv v$), we simplify further to obtain

$$\bar{v}=\frac{1}{1+q_1}v. \tag{B.9}$$

## Appendix C. Derivation of an expression for the spreading

Here we derive expressions for the spreading of the neurofilament transport wave based on the six-state, four-state and two-state models. For the six-state model in equation (15), we find the spread of the neurofilament distribution

$$\sigma^2(t)\equiv\langle x^2(t)\rangle-\langle x(t)\rangle^2 \tag{C.1}$$

by setting up the equation of motion for $\langle x^2(t)\rangle$, i.e.

$$\frac{\rm d}{{\rm d}t}\langle x^2(t)\rangle=2v_{\rm a}M_{\rm a}+2v_{\rm r}M_{\rm r}, \tag{C.2}$$

with

$$M_{\rm a,r,a0,r0,ap,rp}(t)=\int_{-\infty}^{\infty}x\,P_{\rm a,r,a0,r0,ap,rp}(x,t)\,{\rm d}x. \tag{C.3}$$

We then derive the closed set of equations

$$\begin{aligned}
\frac{\rm d}{{\rm d}t}M_{\rm a}&=v_{\rm a}\hat{P}_{\rm a}-\gamma_{10}M_{\rm a}+\gamma_{01}M_{\rm a0}\\
\frac{\rm d}{{\rm d}t}M_{\rm r}&=v_{\rm r}\hat{P}_{\rm r}-\gamma_{10}M_{\rm r}+\gamma_{01}M_{\rm r0}\\
\frac{\rm d}{{\rm d}t}M_{\rm a0}&=-\left(\gamma_{01}+\gamma_{\rm ar}+\gamma_{\rm off}\right)M_{\rm a0}+\gamma_{10}M_{\rm a}+\gamma_{\rm ra}M_{\rm r0}+\gamma_{\rm on}M_{\rm ap}\\
\frac{\rm d}{{\rm d}t}M_{\rm r0}&=-\left(\gamma_{01}+\gamma_{\rm ra}+\gamma_{\rm off}\right)M_{\rm r0}+\gamma_{10}M_{\rm r}+\gamma_{\rm ar}M_{\rm a0}+\gamma_{\rm on}M_{\rm rp}\\
\frac{\rm d}{{\rm d}t}M_{\rm ap}&=\gamma_{\rm off}M_{\rm a0}-\left(\gamma_{\rm ar}+\gamma_{\rm on}\right)M_{\rm ap}+\gamma_{\rm ra}M_{\rm rp}\\
\frac{\rm d}{{\rm d}t}M_{\rm rp}&=\gamma_{\rm off}M_{\rm r0}-\left(\gamma_{\rm ra}+\gamma_{\rm on}\right)M_{\rm rp}+\gamma_{\rm ar}M_{\rm ap}.
\end{aligned} \tag{C.4}$$

Next, we split this system of equations into the following set of equations:

$$\begin{aligned}
\frac{\rm d}{{\rm d}t}s&=\bar{v}-\gamma_{10}s+\gamma_{01}s_0\\
\frac{\rm d}{{\rm d}t}s_0&=-\left(\gamma_{01}+\gamma_{\rm off}\right)s_0+\gamma_{10}s+\gamma_{\rm ra}M_{\rm r0}+\gamma_{\rm on}s_{\rm p}\\
\frac{\rm d}{{\rm d}t}s_{\rm p}&=\gamma_{\rm off}s_0-\gamma_{\rm on}s_{\rm p}
\end{aligned} \tag{C.5}$$

for the symmetric variables

$$\begin{aligned}
s&=M_{\rm a}+M_{\rm r}\\
s_0&=M_{\rm a0}+M_{\rm r0}\\
s_{\rm p}&=M_{\rm ap}+M_{\rm rp},
\end{aligned} \tag{C.6}$$

and the following set of equations:

$$\begin{aligned}
\frac{\rm d}{{\rm d}t}d&=\bar{v}_d-\gamma_{10}d+\gamma_{01}d_0\\
\frac{\rm d}{{\rm d}t}d_0&=-\left(\gamma_{01}+\gamma_{\rm off}+\gamma_{\rm rev}\right)d_0+\gamma_{\rm on}d_{\rm p}+\gamma_{10}d+\bar{\gamma}_{\rm rev}s_0\\
\frac{\rm d}{{\rm d}t}d_{\rm p}&=\gamma_{\rm off}d_0-\left(\gamma_{\rm on}+\gamma_{\rm rev}\right)d_{\rm p}+\bar{\gamma}_{\rm rev}s_{\rm p}
\end{aligned} \tag{C.7}$$

with $\bar{\gamma}_{\rm rev}=\gamma_{\rm ra}-\gamma_{\rm ar}$ for the asymmetric variables

$$\begin{aligned}
d&=M_{\rm a}-M_{\rm r}\\
d_0&=M_{\rm a0}-M_{\rm r0}\\
d_{\rm p}&=M_{\rm ap}-M_{\rm rp}.
\end{aligned} \tag{C.8}$$

Focussing on long-term solutions (see appendix A) with movement and spread linear in time, we make the ansatz

$$\begin{aligned}
s(t)&=\alpha+\beta t\\
s_0(t)&=\alpha_0+\beta_0 t\\
s_{\rm p}(t)&=\alpha_{\rm p}+\beta_{\rm p}t\\
d(t)&=\delta+\epsilon t\\
d_0(t)&=\delta_0+\epsilon_0 t\\
d_{\rm p}(t)&=\delta_{\rm p}+\epsilon_{\rm p}t.
\end{aligned} \tag{C.9}$$

The resulting set of linear equations for the coefficients $\alpha,\beta,\delta$ and $\epsilon$ can be solved (but is cumbersome) to yield the expressions

$$\frac{\rm d}{{\rm d}t}\langle x(t)\rangle=\bar{v}=\frac{1}{\gamma_{\rm rev}}\frac{1}{1+q_1(1+q_2)}\left(\gamma_{\rm ra}v_{\rm a}+\gamma_{\rm ar}v_{\rm r}\right) \tag{C.10}$$

$$\begin{aligned}
\frac{\rm d}{{\rm d}t}\sigma^2(t)=&\frac{2\bar{v}^2q_1}{1+q_1(1+q_2)}\left(\frac{q_2}{\gamma_{\rm on}}+\frac{(1+q_2)^2}{\gamma_{01}}\right)\\
&+\frac{2\gamma_{\rm ar}\gamma_{\rm ra}}{\gamma_{\rm rev}^2}\frac{1}{\gamma_{10}}\frac{1}{1+q_1(1+q_2)}\\
&\times\left(1+\frac{\gamma_{01}}{\gamma_{\rm rev}}\frac{\gamma_{\rm on}+\gamma_{\rm rev}}{\gamma_{\rm on}+\gamma_{\rm of}+\gamma_{\rm rev}}\right)(v_{\rm a}-v_{\rm r})^2\,.
\end{aligned} \tag{C.11}$$

For the four-state model in equation (12), which lacks off-track transitions (i.e. $\gamma_{\rm on}=\infty$, $\gamma_{\rm off}=0$), this expression simplifies to

$$\begin{aligned}
\frac{\rm d}{{\rm d}t}\sigma^2(t)=&\frac{2q_1}{\gamma_{01}+\gamma_{10}}\bar{v}^2+2\frac{1}{q_1\left(\gamma_{01}+\gamma_{10}\right)}\\
&\times\frac{\gamma_{\rm ra}\gamma_{\rm ar}}{\gamma_{\rm rev}^2}\left(1+\frac{\gamma_{01}}{\gamma_{\rm rev}}\right)(v_{\rm a}-v_{\rm r})^2,
\end{aligned} \tag{C.12}$$

where $\bar{v}$ is given by equation (B.7).

For the two-state model in equation (7), which lacks reversals and off-track transitions (i.e. $\gamma_{\rm off}=0$, $\gamma_{\rm ra}=\gamma_{\rm ar}=0$ and $v_{\rm a}=v_{\rm r}\equiv v$), we simplify further to obtain

$$\frac{\rm d}{{\rm d}t}\sigma^2(t)=\frac{2q_1}{\gamma_{01}+\gamma_{10}}\bar{v}^2=\frac{2\gamma_{01}\gamma_{10}}{\left(\gamma_{01}+\gamma_{10}\right)^3}v^2. \tag{C.13}$$

## Appendix D. Derivation of an expression for the pause duration distribution

Here we derive an expression for the pause duration distributions for the six-state model in equation (15). First, we lump the anterograde and retrograde moving states into a single moving state given by

$$P_1(t)\equiv\int_{-\infty}^{\infty}\left(P_{\rm a}(x,t)+P_{\rm r}(x,t)\right){\rm d}x. \tag{D.1}$$

Similarly, we lump the anterograde and retrograde pausing states into single on-track and off-track pausing states given by

$$P_2(t) \equiv \int_{-\infty}^{\infty} (P_{\rm ap}(x,t) + P_{\rm rp}(x,t))\,{\rm d}x$$
$$P_3(t) \equiv \int_{-\infty}^{\infty} (P_{\rm a0}(x,t) + P_{\rm r0}(x,t))\,{\rm d}x. \tag{D.2}$$

Thus, the equations of motion are obtained as

$$\frac{{\rm d}P_1(t)}{{\rm d}t} = -\gamma_{10}P_1 + \gamma_{01}P_2 \tag{D.3}$$
$$\frac{{\rm d}P_2(t)}{{\rm d}t} = -\gamma_{01}P_2 + \gamma_{10}P_1 + \gamma_{\rm on}P_3 - \gamma_{\rm off}P_2 \tag{D.4}$$
$$\frac{{\rm d}P_3(t)}{{\rm d}t} = \gamma_{\rm off}P_2 - \gamma_{\rm on}P_3. \tag{D.5}$$

### *D.1 Pause duration distributions for all pauses*

A pause begins when a neurofilament switches from a moving state into an on-track pausing state and ends when it switches back (figure 4). The time elapsed between the start and end of the pause is the pause duration. Hence, the first term on the right-hand side of equation (D.3) and the second term on the right-hand side of equation (D.4) must be removed to describe the pausing kinetics, i.e.

$$\frac{{\rm d}P_1(t)}{{\rm d}t} = \gamma_{01}P_2 \tag{D.6}$$
$$\frac{{\rm d}P_2(t)}{{\rm d}t} = -\gamma_{01}P_2 + \gamma_{\rm on}P_3 - \gamma_{\rm off}P_2 \tag{D.7}$$
$$\frac{{\rm d}P_3(t)}{{\rm d}t} = \gamma_{\rm off}P_2 - \gamma_{\rm on}P_3. \tag{D.8}$$

Using the obvious conservation law $P_1 + P_2 + P_3 = 1$, we eliminate $P_3$ and find the following closed set of equations for $P_1$ and $P_2$:

$$\frac{{\rm d}P_2(t)}{{\rm d}t} = -(\gamma_{01} + \gamma_{\rm on} + \gamma_{\rm off})P_2 + \gamma_{\rm on}P_1 + \gamma_{\rm on}$$
$$\frac{{\rm d}P_1(t)}{{\rm d}t} = \gamma_{01}P_2. \tag{D.9}$$

The solution of this linear set of equations reads as

$$P_1(t) = 1 + A\exp(\lambda_+ t) + B\exp(\lambda_- t)) \tag{D.10}$$

with

$$\lambda_\pm = -\frac{1}{2}(\gamma_{01} + \gamma_{\rm on} + \gamma_{\rm off}) \pm \frac{1}{2}\sqrt{(\gamma_{01} + \gamma_{\rm on} + \gamma_{\rm off})^2 - 4\gamma_{01}\gamma_{\rm on}}$$
$$A = \frac{\gamma_{01} + \lambda_-}{\lambda_+ - \lambda_-}$$
$$B = -(A+1). \tag{D.11}$$

To get the pause duration distribution for a given state, we must be sure to start in that state. Thus, we use the following initial conditions:

$$P_1(0) = 0$$
$$P_2(0) = 1 \tag{D.12}$$
$$P_3(0) = 0,$$

stating that at the beginning of a pause the neurofilament is in the on-track pausing state. The probability of finding a neurofilament in any one of the pausing states is given by $P_4(t) \equiv P_2(t) + P_3(t) = 1 - P_1(t)$ since $P_1 + P_2 + P_3 = 1$. The probability density of pausing times durations is thus obtained as

$$\rho(t) \equiv -\frac{\rm d}{{\rm d}t}P_4(t) = \frac{\rm d}{{\rm d}t}P_1(t)$$
$$= A\lambda_+\exp(\lambda_+ t) + B\lambda_-\exp(\lambda_- t), \tag{D.13}$$

which is an exact answer.

### *D.2 Pause duration distributions for off-track pauses*

Off-track pauses start when a neurofilament switches from an on-track pausing state to an off-track pausing state and end when it switches back. Hence, in this case we have to remove the fourth term on the right-hand side of equation (D.4) and the first term on the right-hand side of equation (D.5), decoupling $P_3$ from the other equations, i.e.

$$\frac{{\rm d}P_3(t)}{{\rm d}t} = -\gamma_{\rm on}P_3(t). \tag{D.14}$$

With the initial condition $P_3(0) = 1$, i.e. the neurofilament is initially in the off-track pausing state, the distribution of pause times is obtained as

$$\rho_{\rm off}(t) = -\frac{{\rm d}P_3(t)}{{\rm d}t} = \gamma_{\rm on}\exp(-\gamma_{\rm on}t). \tag{D.15}$$

### *D.3 Pause duration distributions for on-track pauses*

On-track pauses start when a neurofilament switches to an on-track pausing state from either a moving state or an off-track pausing state and end when it switches back. Hence, in this case we have to remove the second and third terms on the right-hand side of equation (D.4) and the first term on the right-hand side of equation (D.5), leading to

$$\frac{{\rm d}P_2(t)}{{\rm d}t} = -(\gamma_{\rm off} + \gamma_{01})P_2(t). \tag{D.16}$$

With the initial condition $P_2(0) = 1$, i.e. the neurofilament is starting the pause in the on-track pausing state, the distribution of pause times is obtained as

$$\rho_{\rm on}(t) = -\frac{{\rm d}P_2(t)}{{\rm d}t}$$
$$= (\gamma_{\rm off} + \gamma_{01})\exp(-(\gamma_{\rm off} + \gamma_{01})t). \tag{D.17}$$

## References


[1] Tytell M, Black M M, Garner J A and Lasek R J 1981 Axonal transport: each major rate component reflects the movement of distinct macromolecular complexes *Science* **214** 179–81

[2] Brown A 2003 Axonal transport of membranous and nonmembranous cargoes: a unified perspective *J. Cell Biol.* **160** 817–21

[3] Lasek R J, Paggi P and Katz M J 1992 Slow axonal transport mechanisms move neurofilaments relentlessly in mouse optic axons *J. Cell Biol.* **117** 607–16

[4] Nixon R A 1998 The slow axonal transport of cytoskeletal proteins *Curr. Opin. Cell Biol.* **10** 87–92

[5] Brown A 2003 Live-cell imaging of slow axonal transport in cultured neurons *Methods Cell Biol.* **71** 305–23

[6] Yan Y and Brown A 2005 Neurofilament polymer transport in axons *J. Neurosci.* **25** 7014–21
[7] Wang L, Ho C L, Sun D, Liem R K and Brown A 2000 Rapid movement of axonal neurofilaments interrupted by prolonged pauses *Nature Cell Biol.* **2** 137–41
[8] Roy S, Coffee P, Smith G, Liem R K, Brady S T and Black M M 2000 Neurofilaments are transported rapidly but intermittently in axons: implications for slow axonal transport *J. Neurosci.* **20** 6849–61
[9] Wang L and Brown A 2001 Rapid intermittent movement of axonal neurofilaments observed by fluorescence photobleaching *Mol. Biol. Cell* **12** 3257–67
[10] Uchida A and Brown A 2004 Arrival, reversal, and departure of neurofilaments at the tips of growing axons *Mol. Biol. Cell* **15** 4215–25
[11] Trivedi N, Jung P and Brown A 2007 Neurofilaments switch between distinct mobile and stationary states during their transport along axons *J. Neurosci.* **27** 507–16
[12] Brown A 2000 Slow axonal transport: stop and go traffic in the axon *Nature Rev. Mol. Cell. Biol.* **1** 153–6
[13] Brown A, Wang L and Jung P 2005 Stochastic simulation of neurofilament transport in axons: the 'stop-and-go' hypothesis *Mol. Biol. Cell* **16** 4243–55
[14] Hoffman P N, Lasek R J, Griffin J W and Price D L 1983 Slowing of the axonal transport of neurofilament proteins during development *J. Neurosci.* **3** 1694–700
[15] Hoffman P N, Griffin J W, Gold B G and Price D L 1985 Slowing of neurofilament transport and the radial growth of developing nerve fibers *J. Neurosci.* **5** 2920–9
[16] Watson D F, Hoffman P N, Fittro K P and Griffin J W 1989 Neurofilament and tubulin transport slows along the course of mature motor axons *Brain Res.* **477** 225–32
[17] Xu Z and Tung V W 2001 Temporal and spatial variations in slow axonal transport velocity along peripheral motoneuron axons *Neuroscience* **102** 193–200
[18] Archer D R, Watson D F and Griffin J W 1994 Phosphorylation-dependent immunoreactivity of neurofilaments and the rate of slow axonal transport in the central and peripheral axons of the rat dorsal root ganglion *J. Neurochem.* **62** 1119–25
[19] Sanchez I, Hassinger L, Sihag R K, Cleveland D W, Mohan P and Nixon R A 2000 Local control of neurofilament accumulation during radial growth of myelinating axons *in vivo*: selective role of site-specific phosphorylation *J. Cell Biol.* **151** 1013–24
[20] Ackerley S, Grierson A J, Brownlees J, Thornhill P, Anderton B H, Leigh P N, Shaw C E and Miller C C 2000 Glutamate slows axonal transport of neurofilaments in transfected neurons *J. Cell Biol.* **150** 165–76
[21] Ackerley S, Thornhill P, Grierson A J, Brownlees J, Anderton B H, Leigh P N, Shaw C E and Miller C C J 2003 Neurofilament heavy chain side arm phosphorylation regulates axonal transport of neurofilaments *J. Cell Biol.* **161** 489–95
[22] Blum J J and Reed M C 1989 A model for slow axonal transport and its application to neurofilamentous neuropathies *Cell Motil Cytoskeleton* **12** 53–65
[23] Craciun G, Brown A and Friedman A 2005 A dynamical system model of neurofilament transport in axons *J. Theor. Biol.* **237** 316–22
[24] Müller M J I, Klumpp S and Lipowsky R 2008 Tug-of-war as a cooperative mechanism for bidirectional cargo transport by molecular motors *Proc. Natl Acad. Sci.* **105** 4609–14
[25] Xu Z and Tung V W 2000 Overexpression of neurofilament subunit m accelerates axonal transport of neurofilaments *Brain Res.* **866** 326–32
[26] Millecamps S, Gowing G, Corti O, Mallet J and Julien J-P 2007 Conditional nf-l transgene expression in mice for *in vivo* analysis of turnover and transport rate of neurofilaments *J. Neurosci.* **27** 4947–56
[27] Shah J V, Flanagan L A, Janmey P A and Leterrier J F 2000 Bidirectional translocation of neurofilaments along microtubules mediated in part by dynein/dynactin *Mol. Biol. Cell* **11** 3495–508
[28] Xia C-H, Roberts E A, Her L-S, Liu X, Williams D S, Cleveland D W and Goldstein L S B 2003 Abnormal neurofilament transport caused by targeted disruption of neuronal kinesin heavy chain kif5a *J. Cell Biol.* **161** 55–66
[29] Helfand B T, Loomis P, Yoon M and Goldman R D 2003 Rapid transport of neural intermediate filament protein *J. Cell Sci.* **116** 2345–59
[30] Wagner O I, Ascaño J, Tokito M, Leterrier J-F, Janmey P A and Holzbaur E L F 2004 The interaction of neurofilaments with the microtubule motor cytoplasmic dynein *Mol. Biol. Cell* **15** 5092–100
[31] Francis F, Roy S, Brady S T and Black M M 2005 Transport of neurofilaments in growing axons requires microtubules but not actin filaments *J. Neurosci. Res.* **79** 442–50
[32] He Y, Francis F, Myers K A, Yu W, Black M M and Baas P W 2005 Role of cytoplasmic dynein in the axonal transport of microtubules and neurofilaments *J. Cell Biol.* **168** 697–703
[33] Gross S P 2004 Hither and yon: a review of bi-directional microtubule-based transport *Phys. Biol.* **1** R1–11
[34] Gross S P 2003 Dynactin: coordinating motors with opposite inclinations *Curr. Biol.* **13** R320–2
[35] Welte M A 2004 Bidirectional transport along microtubules *Curr. Biol.* **14** R525–37
[36] Xu Z, Marszalek J R, Lee M K, Wong P C, Folmer J, Crawford T O, Hsieh S T, Griffin J W and Cleveland D W 1996 Subunit composition of neurofilaments specifies axonal diameter *J. Cell Biol.* **133** 1061–9
[37] Perrot R, Berges R, Bocquet A and Eyer J 2008 Review of the multiple aspects of neurofilament functions, and their possible contribution to neurodegeneration *Mol. Neurobiol.* **38** 27–65
[38] Uchida A, Alami N H and Brown A 2009 in preparation